Non-adiabatic effects in F + CHD_3 reactive scattering

Juliana Palma and Uwe Manthe

Citation: The Journal of Chemical Physics **146**, 214117 (2017); doi: 10.1063/1.4984593
View online: http://dx.doi.org/10.1063/1.4984593
View Table of Contents: http://aip.scitation.org/toc/jcp/146/21
Published by the American Institute of Physics

Non-adiabatic effects in F + CHD_3 reactive scattering

Juliana Palma[1,a)] and Uwe Manthe[2,b)]
[1]*Departamento de Ciencia y Tecnología, Universidad Nacional de Quilmes, Sáenz Peña 352, Bernal B1876BXD, Argentina*
[2]*Theoretische Chemie, Fakultät für Chemie, Universität Bielefeld, Universitätsstr. 25, D-33615 Bielefeld, Germany*

(Received 15 April 2017; accepted 16 May 2017; published online 7 June 2017)

The effect of non-adiabatic transitions on the $F(^2P) + CHD_3(\nu_1) \rightarrow DF + CHD_2$ and $F(^2P) + CHD_3(\nu_1) \rightarrow HF + CD_3$ reactions is investigated. The dynamics of the nuclei was simulated using trajectory surface hopping and a vibronically and spin-orbit coupled diabatic potential energy matrix. To facilitate the calculations, the fewest switching algorithm of Tully was adapted to the use of a complex diabatic potential energy matrix. For reactions of CHD_3 with ground state fluorine atoms, $F(^2P_{3/2})$, the ratio between the previously computed adiabatic cross sections and the non-adiabatic ones was found to range from 1.4 to 2.1. The actual ratio depends on the translational energy and the initial vibrational state of CHD_3. The total reactivity of $CHD_3(\nu_1 = 1)$ was found to be always larger than that of $CHD_3(\nu_1 = 0)$ mainly because of the increase in the cross sections for the HF + CD_3 channel. Thus, the inclusion of non-adiabatic transitions in the theoretical treatment cannot resolve the existing disagreement between theory and experiment. Cross sections for the reaction of CHD_3 with spin-orbit excited fluorine atoms, $F(^2P_{1/2})$, were found to be significantly smaller than the ones for reaction with $F(^2P_{3/2})$. *Published by AIP Publishing.* [http://dx.doi.org/10.1063/1.4984593]

I. INTRODUCTION

Reactions of methane with different atoms are benchmark examples of polyatomic reactive processes which have been extensively studied (see, e.g., Refs. 1–18 for prominent examples). Among the different reactions, the ones involving methane or its isotopomers and fluorine serve as examples of reactive processes with an early transition state and a very low barrier. They have been thoroughly investigated in recent years, both experimentally[1–3,19–35] and theoretically.[15,16,36–63] In particular, the F + CHD_3 → DF + CHD_2/HF + CD_3 system has attracted a lot of attention because of the counter-intuitive findings of the cross-beam experiments of Liu and co-workers.[3] They noticed that the excitation of the C–H stretching vibration, ν_1, suppresses the total reactivity and favors the DF + CHD_2 channel over the HF + CD_3 channel. The effect is dramatic at low energies, 1.0 and 3.6 kcal/mol, where the reactivity of $CHD_3(\nu_1 = 1)$ was reported to be 10 times smaller than that of $CHD_3(\nu_1 = 0)$. Later on Yang *et al.* reported that the effect is moderate at 9.0 kcal/mol with just 26% of reduction in total reactivity for the DF + CHD_2 channel[33] and 33.4% for HF + CD_3.[34]

Existing theoretical studies cannot explain the counter-intuitive experimental results. Quasi-classical trajectory (QCT) calculations[47,48] based on a potential energy surface (PES) developed by Czakó, Shepler, Braams, and Bowman (CSBB-PES)[15] found that excitation of the C–H stretching vibration diminishes the yield of HF + CD_3 in favor of DF + CHD_2 at very low collisional energies. However, the total reactivity was observed to increase upon excitation. Further QCT calculations[60] and reduced dimensionality (RD) quantum mechanical computations[16] performed on a more accurate PES, the Palma, Westermann, Eisfeld and Manthe (PWEM)-PES,[58–60] that explicitly accounted for spin-orbit (SO) and vibronic coupling could not confirm the findings of Czakó *et al.* Contradicting Liu's experiments, these calculations found that the excitation of the ν_1 vibration increases the production of HF + CD_3 in comparison with the ground state reaction. The consistency between the results obtained with Reduced dimensionality-Quantum mechanics (RD-QM) and QCT calculations strongly suggests that differences between these theoretical predictions and the experimental results of Liu and co-workers are neither caused by using classical mechanics nor by fixing some degrees of freedom of the reactive system.

Considering reactions of fluorine and chlorine atoms with closed shell molecules, there are always six low-lying electronic states in the entrance channel. Four of these states are degenerate asymptotically and correlate with the $^2P_{3/2}$ level of the halogen atom. The other two electronic states are degenerate to each other and asymptotically correlate to the spin-orbit excited $^2P_{1/2}$ level. The effect of vibronic and SO coupling on reactivity was investigated in detail for the reactions of halogens with hydrogen molecules.[64–69] Non-adiabatic transitions were found to play an important role in F + H_2 collisions.[67,68] Moreover, Born-Oppenheimer forbidden processes were found to be dominating at very low translational energies.[69]

In contrast to the detailed studies available for the triatomic systems, the influence of non-adiabatic transitions on reactions between halogen atoms and methane has not been adequately investigated yet. To the best of our knowledge, the only theoretical study on the subject was performed by Clary

a)Electronic mail: juliana@unq.edu.ar
b)Electronic mail: uwe.manthe@uni-bielefeld.de

and co-workers, who employed a two dimensional quantum mechanical model to investigate the Cl + CH_4 system.[70] The present work studies the F + CHD_3 → DF + CHD_2/HF + CD_3 reactions using a quasi-classical trajectory surface hopping (SH) approach. The calculations employ a set of vibronically and spin-orbit coupled diabatic PESs[58,59] to describe the dynamics in the entrance channel of the reaction and switch to a single adiabatic PES, the CSBB-PES, on the products side.[60] The surface hopping approach used in the calculations is based on the fewest switching algorithm proposed by Tully,[71] adjusted to take into account the fact that a complex diabatic potential energy matrix is employed instead of the set of adiabatic PESs.

The aim of the present work is twofold. First, the question of how non-adiabatic transitions affect the reaction process in general should be answered. The effect of non-adiabatic transitions on reactive cross sections is studied in detail and the validity of the adiabatic approximation is tested. The reactivity of fluorine atoms in the electronic ground state, $^2P_{3/2}$ is compared with the reactivity of spin-orbit excited fluorine atoms in the $^2P_{1/2}$ state. Second, we address the question whether the disagreement between theory and experiment concerning the mode selective chemistry in F + CHD_3 → DF + CHD_2/HF + CD_3 may be caused by the neglect of non-adiabatic effects in the previous theoretical studies.

The rest of the article is organized as follows. Section II describes the procedure implemented to run quasi-classical trajectories with surface hopping using a vibronically and SO coupled diabatic potential energy matrix. Information about the PESs employed in this work is presented in Sec. III. Section IV provides the numerical details required to reproduce the QCT calculations. The results of the calculations are presented and discussed in Sec. V. Section VI closes the article by summarizing the main conclusions.

II. TRAJECTORY SURFACE HOPPING

The dynamical calculations presented here are based on a Hamiltonian in a diabatic representation,

$$\hat{\mathbf{H}} = \hat{\mathbf{T}}_R + \mathbf{V}^d(\mathbf{R}). \tag{1}$$

Here $\mathbf{R}$ denotes the nuclear coordinates, $\hat{\mathbf{T}}_R$ the kinetic energy operator of the nuclei, and $\mathbf{V}^d(\mathbf{R})$ the diabatic potential energy matrix. The elements of $\mathbf{V}^d(\mathbf{R})$ are given by

$$V^d_{nm}(\mathbf{R}) = \left\langle \psi^d_n | \hat{H}_{elec} | \psi^d_m \right\rangle , \tag{2}$$

where the brackets indicate integration with respect to the electronic coordinates, $\hat{H}_{elec}$ is the electronic Hamiltonian, and the ψ^d_n are diabatic electronic wavefunctions. In contrast to the adiabatic electronic wavefunctions ψ^a_k, the diabatic electronic wavefunctions only weakly depend on the nuclear coordinates $\mathbf{R}$.

Mixed quantum-classical calculations employing Tully's fewest switches algorithm[71] require the simultaneous propagation of a wavefunction Ψ describing the state of the electrons and a classical trajectory describing the motion of the nuclei. The electronic wavefunction can alternatively be represented in a diabatic electronic basis,

$$\Psi = \sum_n c^d_n \psi^d_n , \tag{3}$$

or an adiabatic one

$$\Psi = \sum_k c^a_k \psi^a_k . \tag{4}$$

Diabatic and adiabatic representations are related by a unitary transformation matrix $\mathbf{U}$, with $U_{nk} = \langle \psi^d_n | \psi^a_k \rangle$, so that

$$\psi^a_k = \sum_n U_{nk} \psi^d_n \tag{5}$$

and

$$c^d_n = \sum_k U_{nk} c^a_k, \quad c^a_k = \sum_n U^*_{nk} c^d_n. \tag{6}$$

If the Hamiltonian in diabatic representation is known, the transformation matrix and the adiabatic potential energy surfaces $V^a_k(\mathbf{R})$ can easily be obtained by diagonalizing the diabatic potential energy matrix $\mathbf{V}^d(\mathbf{R})$,

$$V^d_{nm}(\mathbf{R}) = \sum_k U_{nk}(\mathbf{R}) V^a_k(\mathbf{R}) U^*_{mk}(\mathbf{R}) . \tag{7}$$

It should be noted that the transformation matrix depends on the position of the nuclei.

In Tully's fewest switches algorithm,[71] the propagation of the classical trajectories is governed by the adiabatic PES of the currently populated adiabatic electronic state. Employing a diabatic representation of the electronic wavefunction, the time evolution of c^d_n associated with a trajectory $\mathbf{R}(t)$ is given by

$$i\hbar \dot{c}^d_n = \sum_m V^d_{nm}(\mathbf{R}(t))\, c^d_m(t). \tag{8}$$

Furthermore, the algorithm requires evaluating the probability of jumps from the current adiabatic state to the others. The probability of a jump depends on the time-derivative of the adiabatic populations $|c^a_k|^2$. The adiabatic coefficients c^a_k can be obtained from the diabatic coefficients c^d_n employing Eq. (6). Adapting Tully's original derivation to the present case, the probability of a jump within a small time interval Δt is evaluated as follows. The change in the population of state k, $\Delta|c^a_k|^2$, observed during a time interval Δt is given by

$$\Delta|c^a_k|^2 = 2Re(c^{a*}_k \dot{c}^a_k)\Delta t. \tag{9}$$

Using Eq. (6), the time derivative can be obtained as

$$\dot{c}^a_k = \sum_j \dot{U}^*_{jk} c^d_j + U^*_{jk} \dot{c}^d_j . \tag{10}$$

Expressing the time derivatives of the diabatic coefficients via the time derivate of the adiabatic ones, one finds

$$\begin{aligned} \dot{c}^a_k &= \sum_j \dot{U}^*_{jk} c^d_j + \frac{1}{i\hbar} \sum_{j,l} U^*_{jk} V^d_{jl} c^d_l \\ &= \sum_{j,m} \dot{U}^*_{jk} U_{jm} c^a_m + \frac{1}{i\hbar} \sum_{j,l,m} U^*_{jk} V^d_{jl} U_{lm} c^a_m \\ &= \sum_{j,m} \dot{U}^*_{jk} U_{jm} c^a_m + \frac{1}{i\hbar} V^a_k c^a_k . \end{aligned} \tag{11}$$

The last step in the above rearrangement employed Eq. (7) and the fact that the transformation matrix is unitary. Inserting Eq. (11) into Eq. (9) and replacing $\Delta U^*_{jk} = \dot{U}^*_{jk} \Delta t$, we obtain

$$\Delta|c^a_k|^2 = \sum_m 2Re\left(c^a_m c^{a*}_k \sum_j \Delta U^*_{jk} U_{jm} \right). \tag{12}$$

Since for unitary $\mathbf{U}$,

$$Re\left(\sum_j \Delta U^*_{jk} U_{jm}\right) = -Re\left(\sum_j \Delta U^*_{jm} U_{jk}\right), \tag{13}$$

the above equation can be cast into the form

$$\Delta|c^a_k|^2 = \sum_{m\neq k} b_{km}, \tag{14}$$

where

$$b_{km} = 2Re\left(c^a_m c^{a*}_k \sum_j \Delta U^*_{jk} U_{jm}\right) \tag{15}$$

and

$$b_{km} = -b_{mk}\ . \tag{16}$$

According to the definition of Eq. (15), b_{km} measures the change observed in the population of the adiabatic state k in the interval Δt because of transitions from state m. A positive value of b_{km} indicates net population transference from state m to state k. It should be noted that b_{km} defined by Eq. (15) is related but is not exactly the same as b_{km} of Eq. (14) of Ref. 71, since the later measures a rate of population change instead of the net change occurred in the interval Δt.

The fewest switching algorithm proposes to minimize the number of jumps between electronic states while maintaining the correct statistical distribution of state populations when a swarm of trajectories is considered. To achieve this, each trajectory is propagated along a single adiabatic PES until a sudden jump of electronic state occurs. To fulfill with the requirement of a minimum amount of jumps, a transition from current state m to an alternative state k during the interval Δt is not allowed for $b_{km} < 0$, while it is allowed with probability

$$p_{km} = b_{km}/|c^a_m|^2, \tag{17}$$

for $b_{km} > 0$.

Jumps between adiabatic PESs are associated with sudden changes of momentum in the trajectory. In the original algorithm, only real electronic wavefunctions were considered and the momentum change $\Delta\mathbf{p}$ induced by the transition was assumed to lie along the non-adiabatic coupling vector

$$\mathbf{d}^a_{km} = \langle\psi^a_k|\nabla_R\psi^a_m\rangle = \sum_n U^*_{nk}\nabla_R U_{nm}. \tag{18}$$

In the present case, however, the adiabatic wave functions and therefore also the coupling vectors are complex and further considerations are required. The momentum jump approximation can be analyzed in terms of the mixed quantum-classical Liouville theory of Kapral and Ciccotti.[72] Employing the stochastic interpretation of Ref. 73, which propagates a electronic density matrix $\boldsymbol{\rho}$ along with each trajectory, the transitions between adiabatic electronic states are described as two step processes: $\rho_{kk} \rightarrow \rho_{km}$ (or ρ_{mk}) $\rightarrow \rho_{mm}$. Each of these transitions causes a change in the classical momenta. In the limit of small momentum changes, the resulting total momentum change associated with the transition from the adiabatic electronic state m to state k is given by

$$\Delta\mathbf{p}_{km} = \mathbf{S}_{km} + \mathbf{S}^*_{km}, \tag{19}$$

where

$$\mathbf{S}_{km} = \frac{(E_k - E_m)}{2(\mathbf{d}^a_{km}\cdot\mathbf{v})}\mathbf{d}^a_{km} \tag{20}$$

and $\mathbf{v} = \dot{\mathbf{R}}$ is the velocity vector of the trajectory. Thus, the momentum change is given by the real vector

$$\Delta\mathbf{p}_{km} = \frac{(E_k - E_m)}{|\mathbf{d}^a_{km}\cdot\mathbf{v}|^2} Re\left[\left(\mathbf{d}^{a*}_{km}\cdot\mathbf{v}\right)\mathbf{d}^a_{km}\right]. \tag{21}$$

It has to be noted that Eq. (21) is accurate only in the limit of $|\Delta\mathbf{p}_{km}| \ll |\mathbf{p}|$. Thus, $\Delta\mathbf{p}_{km}$ given by Eq. (21) is only employed to determine the direction of the momentum change.

The magnitude of the change is determined by requiring that the energy of the trajectory before and after the jump is the same. To this end, the momentum vector before the jump, $\mathbf{p}$, is decomposed into a vector parallel to the direction of the momentum change, $\mathbf{p}_\parallel$, and a vector perpendicular to that direction, $\mathbf{p}_\perp$,

$$\mathbf{p} = \mathbf{p}_\parallel + \mathbf{p}_\perp. \tag{22}$$

Upon electronic transition from state m to state k, $\mathbf{p}_\parallel$ is scaled by a factor λ so that the new momentum reads

$$\mathbf{p}(\lambda) = \lambda\cdot\mathbf{p}_\parallel + \mathbf{p}_\perp. \tag{23}$$

The value of λ is chosen so that the change in the kinetic energy of the nuclei, $T(\mathbf{p}(\lambda)) - T(\mathbf{p})$, compensates the change in the potential energy due to the electronic jump,

$$T(\mathbf{p}(\lambda)) - T(\mathbf{p}) = -(V^a_k(\mathbf{R}) - V^a_m(\mathbf{R})). \tag{24}$$

The expansion of Eq. (24) produces a quadratic equation for λ. If it has no real solutions, the transition is forbidden and the propagation of the nuclei movements is continued on the original surface. Otherwise the transition is allowed and the nuclei movements are propagated on the new surface. In the later case, $\mathbf{p}_\parallel$ is scaled with the value of λ closest to 1.0 since this is in agreement with the small momentum change approximation invoked to obtain $\Delta\mathbf{p}_{km}$ [Eq. (19)].

III. POTENTIAL ENERGY SURFACES AND COUPLINGS

In the entrance channel of the F(^{2}P) + CHD_3 reaction, all six electronic states correlating to the ^{2}P state of the fluorine atom are relevant for the system's dynamics. The six electronic states give rise to three vibronically and spin-orbit coupled different PESs, called SO1, SO2, and SO3 in the following. The SO1 and SO2 PESs asymptotically correlate to the $^2P_{3/2}$ level of fluorine, while the SO3 PES correlates to the spin-orbit excited $^2P_{1/2}$ level. When the system approaches the transition state of the reaction, the energies of the SO2 and SO3 PESs rise significantly compared to the lowest adiabatic PES, SO1. Once the transition state is passed, only the lowest adiabatic PES is relevant for the system's dynamics. The present work employs the vibronically and spin-orbit coupled diabatic potential energy matrix $\mathbf{V}^{(diab)}_{\text{entr}}$ introduced in Refs. 58 and 59 to describe to the entrance channel. The product channel is described using the CSBB-PES,[15] V_{CSBB}, developed by Czakó *et al.*[15]

In Ref. 60, a procedure to smoothly switch between the two domains was introduced. The procedure connects the lowest adiabatic PES $V^{(SO1)}_{\text{entr}}$ obtained by diagonalizating $\mathbf{V}^{(diab)}_{\text{PWEM}}$

with the V_{CSBB} potential using a switching function $S(r)$ which depends on the value r of the smallest of the four H–F distances,

$$V_{\mathrm{PWEM}} = (1 - S(r)) \cdot V_{\mathrm{CSBB}} + S(r) \cdot V_{\mathrm{entr}}^{(SO1)}. \quad (25)$$

The switching occurs between $r_{\mathrm{low}} = 1.5$ Å and $r_{\mathrm{up}} = 1.7$ Å and uses the function

$$S(r) = 10.0\, y(r)^3 - 15.0\, y(r)^4 + 6.0\, y(r)^5,$$
$$y(r) = \frac{r - r_{\mathrm{low}}}{r_{\mathrm{up}} - r_{\mathrm{low}}}. \quad (26)$$

The procedure had to be extended in the present work since a complete diabatic potential energy matrix and not only the lowest adiabatic PES is required in the switching region. To construct a diabatic potential energy matrix $\mathbf{V}_{\mathrm{entr}}^{(diab)}$ in the switching region, first the diabatic-adiabatic transformation matrix $\mathbf{U}_{\mathrm{entr}}$ is calculated by diagonalizing $\mathbf{V}_{\mathrm{entr}}^{(diab)}$,

$$\mathbf{V}_{\mathrm{entr}}^{(diab)} = \mathbf{U}_{\mathrm{entr}} \mathbf{V}_{\mathrm{entr}}^{(adiab)} \mathbf{U}_{\mathrm{entr}}^{\dagger}. \quad (27)$$

Here $\mathbf{V}_{\mathrm{entr}}^{(adiab)}$ is a diagonal matrix with the three adiabatic PESs $V_{\mathrm{entr}}^{(SO1)}$, $V_{\mathrm{entr}}^{(SO2)}$, and $V_{\mathrm{entr}}^{(SO3)}$ as diagonal elements. A new adiabatic potential energy matrix $\mathbf{V}_{\mathrm{PWEM}}^{(adiab)}$, which shows a lowest adiabatic PESs smoothly switching between V_{PWEM} and V_{CSBB}, can be constructed by simply replacing $V_{\mathrm{entr}}^{(SO1)}$ by V_{PWEM} in $\mathbf{V}_{\mathrm{entr}}^{(adiab)}$. The corresponding diabatic potential energy matrix $\mathbf{V}_{\mathrm{PWEM}}^{(diab)}$ is obtained by backtransforming from the adiabatic to the diabatic representation using $\mathbf{U}_{\mathrm{entr}}$,

$$\mathbf{V}_{\mathrm{PWEM}}^{(diab)} = \mathbf{U}_{\mathrm{entr}} \mathbf{V}_{\mathrm{PWEM}}^{(adiab)} \mathbf{U}_{\mathrm{entr}}^{\dagger}. \quad (28)$$

Using the diabatic potential energy matrices $\mathbf{V}_{\mathrm{entr}}^{(diab)}$ and $\mathbf{V}_{\mathrm{PWEM}}^{(diab)}$, our trajectory calculations can include surface hopping in the entrance channel and in the transition state region. In the product channel, no surface hopping takes place and the trajectories are propagated employing V_{CSBB}. Since the electronically excited SO2 and SO3 PESs show increasingly large energies when passing the switching region from the reactant side towards the product side, the trajectories hop to the SO1 PES before reaching the end of the switching region and entering the product channel. This assumption was confirmed by an analysis of the computed trajectories, as detailed below.

IV. COMPUTATIONAL DETAILS

Trajectories were employed to simulate $F(^2P_{3/2})$ + $CHD_3(\nu_1 = 0, 1)$ and $F(^2P_{1/2})$ + $CHD_3(\nu_1 = 0, 1)$ collisions, with either 1.0, 3.6, and 9.0 kcal/mol of collisional energy (E_C). To simulate $F(^2P_{3/2})$ + $CHD_3(\nu_1 = 0, 1)$, one of the adiabatic coefficients c_1^a to c_4^a was initially set to 1.0 while the others were set to 0.0. The number of trajectories starting with c_1^a = 1.0 or c_2^a = 1.0 was the same as the number starting from c_3^a = 1.0 or c_4^a = 1.0. Therefore, the populations of the SO1 and SO2 adiabatic states were exactly the same at the beginning. We run 70 000 trajectories for E_C = 1.0 kcal/mol and 40 000 for E_C = 3.6 or 9.0 kcal/mol, for each initial vibrational state of CHD_3. To simulate $F(^2P_{1/2})$ + $CHD_3(\nu_1 = 0, 1)$, either c_5^a or c_6^a was initially set to 1.0 while the other coefficients were set to 0.0. In this case, we run 40 000 trajectories for each collisional energy and each vibrational state of CHD_3.

The initial separation between the carbon and fluorine atoms was set to $18.90a_0$. The impact parameter was chosen at random from a uniform distribution function between 0 and $8.0a_0$. Therefore, trajectories were weighted according to the selected value of the impact parameter.[74] The initial orientation of CHD_3 was defined by randomly choosing the Euler angles that determine the orientation of its body fixed frame. Standard normal-mode sampling was employed to initialize the vibrational state of CHD_3, either to the ground state or to the $\nu_1 = 1$ excited state. The standard iterative velocity adjustment was employed to set the initial angular momentum of CHD_3 to zero.[74] Trajectories were ended when the collisional fragments were moving away from each other and the distance between them was larger than $15.0a_0$. At the end of each trajectory, the distances between atoms were analyzed to determine if any of the D atoms or the H atom had reacted.

The propagation employed the scheme presented in Sec. II. The probability of jumps between adiabatic surfaces was evaluated every 2.0 fs. Derivatives of the potential, as well as derivatives of the elements of the **U** matrix, were numerically computed. The equations of motion were integrated employing a variable order, variable step Adams method. The conservation of the total energy along the trajectories was checked and typical errors were found to be smaller than 0.04%. However, we occasionally detected trajectories with larger errors. Therefore, we set an upper limit of 0.6% for the maximum acceptable error in the total energy. Any trajectory with an energy error larger than that was discarded from the subsequent computations. We checked that different upper limits, in the range of 0.1%–0.9%, produced the same cross sections within the statistical uncertainty. Also, we sometimes found trajectories for which the integrator was unable to make any further progress because the step size required by the algorithm became too small. These trajectories were stopped and discarded. This problem was never found in calculations performed with a collisional energy of 1.0 kcal/mol and rarely occurs for 3.6 kcal/mol. However, for 9.0 kcal/mol of collisional energy about 1/600 trajectories presented the problem. Finally, as stated in Sec. III, trajectories passing the switching region from the reactant side towards the product side are expected to hop to the SO1 PES before reaching the end of that region. This assumption was fulfilled by all the trajectories with E_C = 1.0 kcal/mol and 3.6 kcal/mol, as well as for trajectories with E_C = 9.0 kcal/mol initiated with CHD_3 in the vibrational ground state. For $F(^2P_{3/2})$ + $CHD_3(\nu_1 = 1)$ collisions with E_C = 9.0 kcal/mol, we found four trajectories moving into the products' channel while still being in the SO2 or SO3 PESs. In the case of $F(^2P_{1/2})$ + $CHD_3(\nu_1 = 1)$ collisions with E_C = 9.0 kcal/mol, this number raises to twelve. All these ill-behaved trajectories eventually go back to the reactants channel. These trajectories were not considered in the calculation of the cross sections.

During the incoming part of the trajectories, the carbon-fluorine distance and the actual adiabatic state were recorded every 2.0 fs. These data were used to estimate the electronic populations as a function of such distance by applying the

following computation. The range of putative values of the C–F distance, $2.5a_0$ to $18.5a_0$, was divided into 16 bins. For each trajectory, we determined the number of samples falling within a given bin. For bins not visited by the trajectory, a occupation probability of zero was assigned to all the electronic states. For a bin visited N_{sample} times, the occupation probability of electronic state SO_α was computed as $N_{SO\alpha}/N_{\text{sample}}$, where N_{SO_α} measures the number of times the trajectory was found in the given bin in state SO_α. The resulting occupation probabilities were finally averaged taking into account all the trajectories, considering the trajectory weighting resulting from the different impact parameters.

V. RESULTS AND DISCUSSION

Cross sections σ_H and σ_D, for which we considered non-adiabatic transitions and were computed using the surface hopping approach described in Sec. II, are presented in Table I. Here σ_H and σ_D refer to the $F(^2P_{3/2}) + CHD_3(\nu_1 = 0, 1) \rightarrow HF + CD_3$ and $F(^2P_{3/2}) + CHD_3(\nu_1 = 0, 1) \rightarrow DF + CHD_2$ reactions, respectively. The values σ_H^{ad} and σ_D^{ad} previously obtained in calculations that considered only the lowest adiabatic PES and neglected non-adiabatic transitions are also shown in the table to facilitate the comparison. In the following, the cross sections σ_H and σ_D will be called non-adiabatic cross sections while σ_H^{ad} and σ_D^{ad} will be called adiabatic cross sections. In Table II, cross sections for the reaction of spin-orbit excited fluorine atoms, $F(^2P_{1/2}) + CHD_3(\nu_1 = 0, 1) \rightarrow HF + CD_3$ and $F(^2P_{1/2}) + CHD_3(\nu_1 = 0, 1) \rightarrow DF + CHD_2$, are given.

In Secs. V A–V C we analyze these results from different points of view. First we discuss the effect of non-adiabatic transitions on reaction probabilities. Then the present results are related to the experimental results of Liu and co-workers. Finally the problem of Zero Point Energy (ZPE) leakage in the low energy range will be discussed.

A. Effect of non-adiabatic transitions

There are two adiabatic surfaces asymptotically correlating with $F(^2P_{3/2})$ but only one of them correlates with the products' channel. If non-adiabatic transitions are completely neglected, the non-adiabatic cross section σ, which considers both PESs, would be half of the size of the adiabatic cross section σ^{ad}, which is computed on the reactive PES only. This straightforward application of the adiabatic approximation would thus imply that $\sigma^{\text{ad}} = 2 \cdot \sigma$. Alternatively, one could assume that transitions between the two degenerate components of the electronic state correlating to $F(^2P_{3/2})$ are fast and that a complete transfer to the reactive adiabatic PES occurs during the approach of the reactants. Employing this assumption, adiabatic and non-adiabatic cross sections would be equal, $\sigma^{\text{ad}} = \sigma$.

The ratios $\sigma_D^{\text{ad}}/\sigma_D$ and $\sigma_H^{\text{ad}}/\sigma_H$ for $\nu_1 = 0$ and 1 are displayed in Fig. 1, as a function of the collisional energy. One immediately finds that the assumption of a fast and complete population transfer to the reactive PES is incorrect. The $\sigma^{\text{ad}}/\sigma$ ratios are always significantly larger than one. In most cases, they are closer to two than to one. Thus, a straightforward application of the adiabatic approximation which completely ignores non-adiabatic transitions generally seems to be the

TABLE II. Cross sections in a_0^2 for $F(^2P_{1/2}) + CHD_3(\nu_1 = 0, 1) \rightarrow DF + CHD_2$ (σ_D) and $F(^2P_{1/2}) + CHD_3(\nu_1 = 0, 1) \rightarrow HF + CD_3$ (σ_H).

	σ_D	σ_H
E_C = 1.0 kcal/mol		
$CHD_3(\nu_1 = 0)$	0.029 ± 0.008	0.016 ± 0.006
$CHD_3(\nu_1 = 1)$	0.025 ± 0.007	0.010 ± 0.005
E_C = 3.6 kcal/mol		
$CHD_3(\nu_1 = 0)$	0.826 ± 0.043	0.272 ± 0.024
$CHD_3(\nu_1 = 1)$	0.746 ± 0.040	0.323 ± 0.026
E_C = 9.0 kcal/mol		
$CHD_3(\nu_1 = 0)$	3.393 ± 0.094	1.393 ± 0.060
$CHD_3(\nu_1 = 1)$	3.593 ± 0.098	1.759 ± 0.071

TABLE I. Cross sections in a_0^2 for $F(^2P_{3/2}) + CHD_3(\nu_1 = 0, 1) \rightarrow DF + CHD_2$ (σ_D) and $F(^2P_{3/2}) + CHD_3$ ($\nu_1 = 0, 1$) $\rightarrow HF + CD_3$ (σ_H). Numbers within parentheses are the values previously obtained considering only the lowest adiabatic PES.

	σ_D (σ_D^{ad})	σ_H (σ_H^{ad})	σ_D/σ_H ($\sigma_D^{\text{ad}}/\sigma_H^{\text{ad}}$)
E_C = 1.0 kcal/mol			
$CHD_3(\nu_1 = 0)$	0.67 ± 0.03 (1.05 ± 0.06)	0.32 ± 0.02 (0.40 ± 0.04)	2.09 ± 0.22 (2.62 ± 0.41)
$CHD_3(\nu_1 = 1)$	0.79 ± 0.04 (1.57 ± 0.07)	1.28 ± 0.05 (4.31 ± 0.15)	0.62 ± 0.06 (0.36 ± 0.03)
E_C = 3.6 kcal/mol			
$CHD_3(\nu_1 = 0)$	7.74 ± 0.15 (14.88 ± 0.20)	3.09 ± 0.10 (5.04 ± 0.12)	2.50 ± 0.13 (2.95 ± 0.11)
$CHD_3(\nu_1 = 1)$	7.56 ± 0.15 (15.88 ± 0.20)	5.12 ± 0.13 (10.73 ± 0.12)	1.48 ± 0.07 (1.48 ± 0.04)
E_C = 9.0 kcal/mol			
$CHD_3(\nu_1 = 0)$	14.07 ± 0.20 (22.68 ± 0.34)	5.74 ± 0.13 (8.06 ± 0.21)	2.45 ± 0.09 (2.81 ± 0.12)
$CHD_3(\nu_1 = 1)$	13.44 ± 0.21 (23.31 ± 0.33)	7.69 ± 0.17 (13.00 ± 0.26)	1.75 ± 0.07 (1.79 ± 0.06)

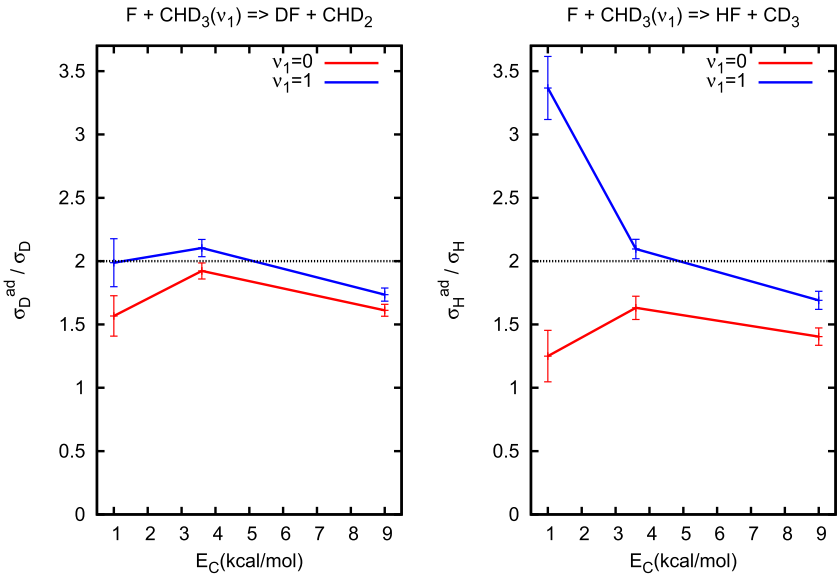

FIG. 1. Ratio between cross sections computed on the lowest adiabatic PES (σ_H^{ad}, σ_D^{ad}) and cross sections considering non-adiabatic transitions (σ_H, σ_D).

better of the two simple models discussed above. However, even this model fails qualitatively for $F(^2P_{3/2}) + CHD_3(\nu_1 = 0) \rightarrow HF + CD_3$.

While for the two larger collision energies, 3.6 and 9.0 kcal/mol, the ratios $\sigma^{\mathrm{ad}}/\sigma$ always take physically reasonable values, some unreasonable results are found at the lowest collision energy, 1.0 kcal/mol. The most extreme result is found for $\sigma_H^{\mathrm{ad}}/\sigma_H$, where the ratio shows a value between 3.0 and 3.5. As discussed below in more detail, we have found that QCT trajectories, either adiabatic or non-adiabatic, have problems with the ZPE leakage. In the low energy range, the problem is severe and renders the results obtained at E_C = 1.0 kcal/mol unreliable. In the following discussion, we concentrate on results at 3.6 and 9.0 kcal/mol which are trustworthy.

Studying Fig. 1 in more detail, one finds that $\sigma_D^{\mathrm{ad}}/\sigma_D$ and $\sigma_H^{\mathrm{ad}}/\sigma_H$ are both smaller for $\nu_1 = 0$ than for $\nu_1 = 1$. This indicates that alternative vibrational states of CHD_3 are influenced in a different way by the non-adiabatic transitions. The difference is larger for the $F(^2P_{3/2}) + CHD_3 \rightarrow HF + CD_3$ reaction than for $F(^2P_{3/2}) + CHD_3 \rightarrow DF + CHD_2$. The second finding is that $\sigma_D^{\mathrm{ad}}/\sigma_D$ as well as $\sigma_H^{\mathrm{ad}}/\sigma_H$ are larger for E_C = 3.6 kcal/mol than for E_C = 9.0 kcal/mol. A smaller ratio of $\sigma^{\mathrm{ad}}/\sigma$ indicates an increased importance of non-adiabatic transitions. We thus find that non-adiabatic transitions are more relevant at higher collision energies.

In principle, increased reactivity in comparison with the expectations of a fully adiabatic process could be explained by a net transfer of electronic population from the repulsive SO2 state to the reactive SO1 state. Figure 2 shows the averaged populations of the electronic states for incoming trajectories as a function of the C–F distance for both $F(^2P_{3/2}) + CHD_3(\nu_1 = 0)$ and $F(^2P_{3/2}) + CHD_3(\nu_1 = 1)$ collisions. Note that the sum of the populations at a given distance d(C–F) equals the probability that an incoming trajectory reaches d(C–F) before

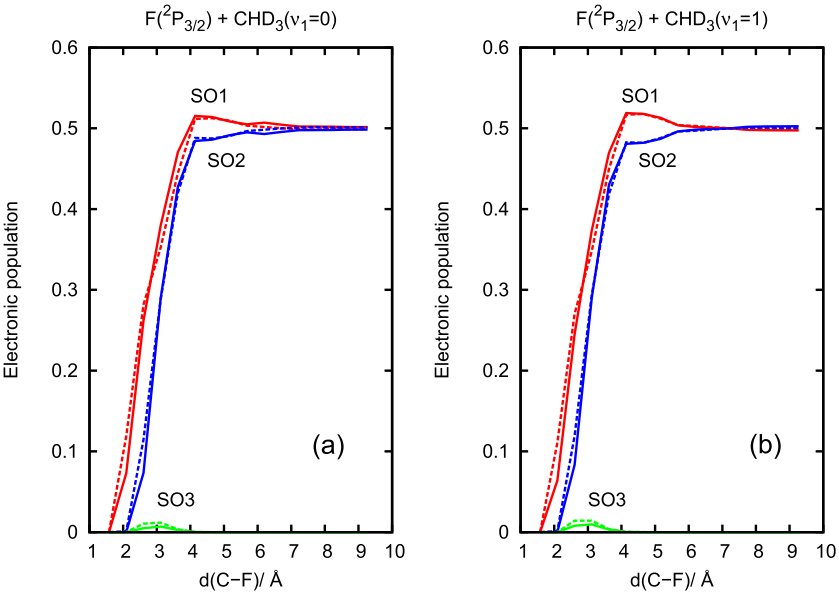

FIG. 2. Populations of the SO adiabatic states for incoming $F(^2P_{3/2}) + CHD_3(\nu_1)$ trajectories as a function of the C–F distance (see text for details). Solid lines are for E_C = 3.6 kcal/mol and dashed lines for E_C = 9.0 kcal/mol.

being reflected towards reactants or products (for a detailed definition see Sec. IV). As expected, in the asymptotic region, the populations of SO1 and SO2 are the same. However, when the collisional partners come close together, there is indeed a net transfer from SO2 to SO1. This process occurs from ≈6 to 3.5 Å, where one can clearly see that what is lost in SO2 appears in SO1. After that, some trajectories are reflected and some others cross towards the product side. This reduces the populations of SO1 and SO2, since Fig. 2 only considers the incoming trajectories. Also, in the strong interaction region, there is a very small but noticeable transfer towards the upper state SO3. The gain in the population of SO1, at the expense of SO2, occurs for both $F(^2P_{3/2}) + CHD_3(\nu_1 = 0)$ and $F(^2P_{3/2}) + CHD_3(\nu_1 = 1)$ collisions and is essentially independent of the collision energy. Besides, the gain is slightly more significant for collisions involving $CHD_3(\nu_1 = 1)$.

If the reaction probabilities were proportional to the probability of being on the reactive PES, the results presented in Fig. 2 would imply that σ_D^{ad}/σ_D and σ_H^{ad}/σ_H should always be smaller than 2.0. Moreover, σ^{ad}/σ should be smaller for $\nu_1 = 1$ than for $\nu_1 = 0$. However, from Fig. 1 one observes that σ^{ad}/σ is always larger for $\nu_1 = 1$ than for $\nu_1 = 0$. Thus, the non-adiabatic transitions affect the reaction process in a complex way. Their impact cannot be understood by only looking at the probability of being on the reactive PES.

Reactive cross sections were also computed for $F(^2P_{1/2}) + CHD_3(\nu_1 = 0, 1)$ collisions and were found to be significantly smaller than for $F(^2P_{3/2}) + CHD_3(\nu_1 = 0, 1)$ (see Table II). An inspection of the electronic populations for this process as a function of the C–F distance, similar to the one presented in Fig. 2, reveals that trajectories initiated on the SO3 state mostly remain on that surface. Only a small fraction of them is transferred to the lower states when they reach the strong interaction region. This leads to the observed reactivity. It is thus concluded that trajectories initiated at the SO3 state make a rather small contribution to the $F(^2P) + CHD_3(\nu_1 = 0, 1) \rightarrow DF + CHD_2$ and $F(^2P) + CHD_3(\nu_1 = 0, 1) \rightarrow HF + CD_3$ reactions.

B. Comparison to experiment

One motivation of the present work was to investigate whether non-adiabatic transitions, which have been neglected in all previous theoretical work, could explain the disagreement between theoretical predictions and experimental findings in the $F(^2P_{3/2}) + CHD_3(\nu_1)$ cross sections. The present calculations indicate that non-adiabatic effects do not alter the σ_D/σ_H branching ratio for $F(^2P_{3/2}) + CHD_3(\nu_1 = 1)$ and only slightly decrease σ_D/σ_H for $F(^2P_{3/2}) + CHD_3(\nu_1 = 0)$ (see Table I). Thus, regarding the DF + CHD_2/HF + CD_3 branching ratio, the present results roughly agree with the previous QCT calculations which neglected non-adiabatic effects and disagree with the experimental findings of Liu and co-workers. In other words, including non-adiabatic transitions in QCT trajectories does not remedy the disagreement between theoretical predictions and experimental findings. The reasons of this discrepancy remain open.

Considering the comparison between experimental and theoretical results, a second point has to be mentioned. The present calculations clearly indicate that the reactive cross sections calculated on the lowest adiabatic PES significantly differs from the "true" cross sections which could be obtained by a calculation properly including non-adiabatic effects. If only data obtained within the adiabatic approximation are available, ignoring non-adiabatic transitions and multiplying σ^{ad} by a correction factor that considers the number of asymptotically degenerate (reactive and non-reactive) PESs are found to be a better approximation than taking uncorrected σ^{ad}.

C. Effect of ZPE leakage in trajectories at 1.0 kcal/mol

In the course of this investigation we analyzed a huge number of trajectories, in order to check that the behavior of the non-adiabatic trajectories was reasonable. This analysis led us to verify that, at E_C = 1.0 kcal/mol, CHD_3 loses a significant fraction of its initial vibrational energy. To perform this analysis, we considered the non-reactive trajectories. At the end of each of such trajectories, we first calculated the kinetic energy of the atoms of CHD_3, in a coordinate frame centered on its center of mass. This accounts for the kinetic energy of the vibrational and rotational motions, K_{vr}. Then, the rotational energy of the fragment was computed as $K_r = \boldsymbol{\omega}^T . \mathbf{I} . \boldsymbol{\omega}$, where vector $\boldsymbol{\omega}$ is the angular velocity of CHD_3 in the center-of-mass frame while $\mathbf{I}$ is the instantaneous inertia matrix. The kinetic energy of the vibrational motion is then obtained as $K_v = K_{vr} - K_r$. Finally the potential energy due to the internal distortions, V, is evaluated by taking the fluorine atom far away from CHD_3, rendering the vibrational energy of the fragment as $E_v = K_v + V$. Since the elements of the inertia matrix fluctuate with time, the energies of rotation and vibration do too, although K_{vr} remains constant. Therefore, in order to obtain meaningful values, we averaged the instantaneous E_v over 100 samples taken at intervals of 2.0 fs. Both, adiabatic and non-adiabatic trajectories were analyzed in the same way.

Figure 3 shows the probability density for the change in the vibrational energy of CHD_3, $\Delta E(CHD_3) = E_{v,final} - E_{v,initial}$, for trajectories corresponding to $\nu_1 = 0$, at 1.0 kcal/mol and 9.0 kcal/mol. The results for $\nu_1 = 1$ are qualitatively similar to those of $\nu_1 = 0$. It is seen that the probability density of $\Delta E(CHD_3)$ changes significantly with the collisional energy. At 9.0 kcal/mol the curves are very thin and almost symmetric around $\Delta E = 0.0$, with the distribution corresponding to non-adiabatic trajectories being somewhat wider than one of the adiabatic trajectories. On the other hand, at 1.0 kcal/mol both curves are rather asymmetric. This is reasonable because positive values of $\Delta E(CHD_3)$ cannot be larger than 1.0 kcal/mol. But the most significant feature is that the two curves present very long tails at negative values that extend beyond −4.0 kcal/mol. The tail is more pronounced for the non-adiabatic trajectories than for the adiabatic ones. The fact that the distributions for 1.0 kcal/mol are wider than those of 9.0 kcal/mol is not surprising. At the higher energy the collisions are direct, so that the collisional partners hardly have time to interact. On the other hand, at low collisional energies, they spend some time in the strong interaction region. Typically, they can remain between 270 fs and 370 fs in configurations with a C–F distance smaller than 3.6 Å. This allows the energy flow from the

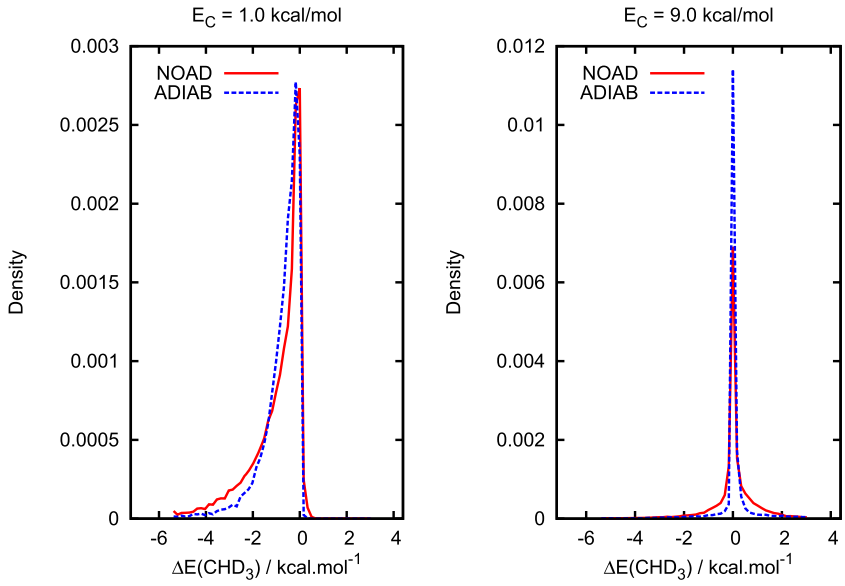

FIG. 3. Probability density for the change in vibrational energy of CHD_3, $\Delta E(CHD_3)$, upon $F(^2P_{3/2})$ + $CHD_3(\nu_1 = 0)$ collisions at 1.0 kcal/mol and 9.0 kcal/mol.

vibrations of CHD_3 to the degrees of freedom that describe the intermolecular motions.

The fact that the curves for the non-adiabatic trajectories are wider than those of the adiabatic trajectories can be rationalized with the following argument. Non-adiabatic transitions to an upper surface are allowed when there is enough kinetic energy along the transition vector. In collisions with ν_1 = 0, there are initially 22.5 kcal/mol in the internal vibrations of CHD_3 while there is 1.0 or 9.0 kcal/mol in the translational motion. Therefore, transitions to an upper surface are more likely to be accepted when they take the energy from the vibrations of CHD_3 than from the translational motion. Clearly this effect is much more marked at 1.0 kcal/mol, where only a small fraction of the total energy is in the relative motion. When the trajectory jumps back to the lowest surface, part of the energy taken from CHD_3 is channeled into the relative motion thus contributing to the ZPE-energy leakage.

In any case, the most important message from this section is the following. Both adiabatic and non-adiabatic trajectories show a significant ZPE-energy leakage at low collisional energies. In such cases, the vibrational energy lost by CHD_3 can even exceed the energy initially put into the translational motion. If the energy lost by CHD_3 along the first half of the reaction is similar or larger than the energy initially put into the relative motion, the reactivity observed in QCT trajectories becomes meaningless. The problem is magnified by the extremely low barrier to the reaction of the F + CHD_3 system, since small energy leaks can have huge effects on reactivity. At higher collisional energies, QCT results are more reliable because the collisions are direct and this leads to much smaller energy leaks. Besides, the energy flow occurs in both directions so that its potentially harmful effect is partially compensated. The good agreement between the results obtained by reduced-dimensional wave packet dynamics and QCT calculations at 3.6 and 9.0 kcal/mol[16] reinforces the idea that quasi-classical trajectories are trustworthy in the medium and high energy ranges.

VI. CONCLUSIONS

We have presented the first theoretical evaluation on the importance of non-adiabatic effects in the F + CHD_3 reactive system. The feasibility of the calculations rests on the existence of a set coupled diabatic potentials developed in previous work. The dynamical calculations were performed by incorporating a surface hopping algorithm into our quasi-classical trajectory code. Our surface hopping algorithm follows the guidelines of the fewest switches method of Tully. However, further developments were required to adapt Tully's method to the complex diabatic potential energy matrix available for this work.

For $F(^2P_{3/2}) + CHD_3(\nu_1)$, with 3.6 or 9.0 kcal/mol of collisional energy, we found that the adiabatic cross sections, σ^{ad}, are larger than the non-adiabatic ones, σ, by a factor that ranges between 1.4 and about 2.1. The actual factor depends on the collisional energy and the vibrational state of CHD_3. As a general rule, the σ^{ad}/σ ratio is larger for $F(^2P_{3/2}) + CHD_3(\nu_1 = 1)$ than for $F(^2P_{3/2})$ + $CHD_3(\nu_1 = 0)$. Moreover, for $F(^2P_{3/2})$ + $CHD_3(\nu_1 = 0)$ it is always smaller than 2.0. Also, as a general rule, the σ^{ad}/σ ratio decreases when increasing the collisional energy. Furthermore we found that the reactivity of electronically excited fluorine atoms, $F(^2P_{1/2})$, is very small compared with that of atoms in the ground electronic state.

As a by-product of the calculations performed in this work we determined that, at low collisional energies, CHD_3 leaks a significant amount of its vibrational energy into the inter-molecular degrees of freedom. Because of that, QCT calculations performed around 1.0 kcal/mol or smaller energies become meaningless.

Finally, when non-adiabatic cross sections for the ground and vibrationally excited states of $CHD_3(\nu_1)$ are compared to each other, it is found that total reactivity increases upon excitation. This enhancement is mainly caused by the increase of reactivity towards the HF + CD_3 product channel. Therefore, the results of the current theoretical study also disagree with the experimental findings of Liu and co-workers. Including non-adiabatic effects in the theoretical treatment does not

resolve the existing discrepancies between theory and experiment. While the reasons for this discrepancy remain unknown, it is reassuring to note that the search for these reasons is driving new investigations on the system. This, in turn, has served to reveal interesting characteristics of its reactivity and has pushed new theoretical developments that can, eventually, be used in other polyatomic systems.

ACKNOWLEDGMENTS

Financial support by the Deutsche Forschungsgemeinschaft is gratefully acknowledged. J.P. is very grateful to the Universidad de Quilmes and CONICET for financial support.

[1] J. Lin, J. Zhou, W. Shiu, and K. Liu, Science **300**, 966 (2003).
[2] W. Shiu, J. Lin, and K. Liu, Phys. Rev. Lett. **92**, 103201 (2004).
[3] W. Zhang, H. Kawamata, and K. Liu, Science **325**, 303 (2009).
[4] Z. H. Kim, H. A. Bechtel, and R. N. Zare, J. Chem. Phys. **117**, 3232 (2002).
[5] R. J. Holiday, C. H. Kwon, C. J. Annesly, and F. F. Crim, J. Chem. Phys. **125**, 133101 (2006).
[6] S. Yan, Y.-T. Wu, B. Zhang, X. F. Yue, and K. Liu, Science **316**, 1723 (2007).
[7] S. Yan, Y. T. Wu, B. Zhang, X. F. Yue, and K. Liu, Proc. Natl. Acad. Sci. U. S. A. **105**, 12667 (2008).
[8] T. Wu, H. J. Werner, and U. Manthe, Science **306**, 2227 (2004).
[9] G. Schiffel and U. Manthe, J. Chem. Phys. **132**, 191101 (2010).
[10] W. Zhang, Y. Zhou, G. Wu, Y. Lu, H. Pan, B. Fu, Q. Shuai, L. Liu, S. Liu, L. Zhang *et al.*, Proc. Natl. Acad. Sci. U. S. A. **107**, 12782 (2010).
[11] S. Liu, J. Chen, Z. Zhang, and D. H. Zhang, J. Chem. Phys. **138**, 011101 (2013).
[12] R. Welsch and U. Manthe, J. Chem. Phys. **141**, 051102 (2014).
[13] R. Welsch and U. Manthe, J. Phys. Chem. Lett. **6**, 338 (2015).
[14] G. Czakó and J. M. Bowman, Science **334**, 343 (2011).
[15] G. Czakó, B. C. Shepler, B. J. Braams, and J. M. Bowman, J. Chem. Phys. **130**, 084301 (2009).
[16] J. Qi, H. Song, M. Yang, J. Palma, U. Manthe, and H. Guo, J. Chem. Phys. **144**, 171101 (2016).
[17] G. Czakó and J. M. Bowman, Proc. Natl. Acad. Sci. U. S. A. **109**, 7997 (2012).
[18] R. Liu, M. Yang, G. Czakó, J. M. Bowman, J. Li, and H. Guo, J. Phys. Chem. Lett. **3**, 3776 (2012).
[19] J. Zhou, J. Lin, W. Shiu, S. C. Pu, and K. Liu, J. Chem. Phys. **119**, 2538 (2003).
[20] J. Zhou, J. Lin, W. Shiu, and K. Liu, J. Chem. Phys. **119**, 4997 (2003).
[21] J. Zhou, J. Lin, and K. Liu, J. Chem. Phys. **119**, 8289 (2003).
[22] J. Zhou, W. Shiu, J. Lin, and K. Liu, J. Chem. Phys. **120**, 5863 (2004).
[23] J. Zhou, J. Lin, and K. Liu, J. Chem. Phys. **121**, 813 (2003).
[24] J. Zhou, W. Shiu, J. Lin, and K. Liu, J. Chem. Phys. **124**, 104309 (2006).
[25] J. Zhou, J. Lin, W. Shiu, and K. Liu, Phys. Chem. Chem. Phys. **8**, 3000 (2006).
[26] B. Zhang, S. Yan, and K. Liu, J. Phys. Chem. A **111**, 9263 (2007).
[27] G. Czakó, Q. Shuai, K. Liu, and J. M. Bowman, J. Chem. Phys. **133**, 131101 (2010).
[28] W. W. Harper, S. A. Nizkorodov, and D. J. Nesbitt, J. Chem. Phys. **113**, 3670 (2000).
[29] W. Shiu, J. J. Lin, K. Liu, M. Wu, and D. H. Parker, J. Chem. Phys. **120**, 117 (2004).
[30] A. Persky, J. Phys. Chem. **100**, 689 (1996).
[31] T. I. Yacovitch, E. Garand, J. B. Kim, C. Hock, T. Theis, and D. M. Neumark, Faraday Discuss. **157**, 399 (2012).
[32] M. Cheng, Y. Feng, Y. Du, Q. Zhu, W. Zheng, G. Czakó, and J. M. Bowman, J. Chem. Phys. **134**, 191102 (2011).
[33] J. Yang, D. Zhang, B. Jiang, D. Dai, G. Wu, D. Zhang, and X. Yang, J. Phys. Chem. Lett. **5**, 1790 (2014).
[34] J. Yang, D. Zhang, Z. Chen, F. Blauert, B. Jiang, D. Dai, G. Wu, D. Zhang, and X. Yang, J. Chem. Phys. **143**, 044316 (2015).
[35] K. Liu, J. Chem. Phys. **142**, 080901 (2015).
[36] D. Troya, J. Millán, I. Baños, and M. González, J. Chem. Phys. **120**, 5181 (2004).
[37] J. Castillo, F. J. Aoiz, L. Bañares, E. Martinez-Nuñez, A. Fernández-Ramos, and S. Vazquez, J. Phys. Chem. A **109**, 8459 (2005).
[38] D. Troya, J. Chem. Phys. **123**, 214305 (2005).
[39] Q. Wang, Z. Cai, and D. Feng, J. Mol. Struct.: THEOCHEM **759**, 31 (2006).
[40] J. Espinosa-García, J. L. Bravo, and C. Rángel, J. Phys. Chem. A **111**, 2761 (2007).
[41] J. C. Corchado and J. Espinosa-García, J. Chem. Phys. **105**, 3152 (1996).
[42] J. C. Corchado and J. Espinosa-García, J. Chem. Phys. **105**, 3160 (1996).
[43] C. Rángel, M. Navarrete, and J. Espinosa-García, J. Phys. Chem. A **109**, 1441 (2005).
[44] J. P. Layfield, A. F. Sweeney, and D. Troya, J. Phys. Chem. A **113**, 4294 (2009).
[45] G. Czakó and J. M. Bowman, Phys. Chem. Chem. Phys. **13**, 8306 (2011).
[46] O. Roberto-Neto, F. B. Machado, and F. R. Ornellas, Chem. Phys. **315**, 27 (2005).
[47] G. Czakó and J. M. Bowman, J. Am. Chem. Soc. **131**, 17534 (2009).
[48] G. Czakó and J. M. Bowman, J. Chem. Phys. **131**, 244302 (2009).
[49] X. Tian, T. Gao, N. He, and Z. Zhang, Mol. Phys. **106**, 2717 (2008).
[50] J. Espinosa-García, J. Chem. Phys. **130**, 054305 (2009).
[51] J. Espinosa-García and J. L. Bravo, J. Phys. Chem. A **112**, 6059 (2008).
[52] J. Espinosa-García, J. Phys. Chem. A **111**, 3497 (2007).
[53] J. Espinosa-García, Chem. Phys. Lett. **488**, 153 (2010).
[54] T. Chu, K. Han, and J. Espinosa-García, J. Chem. Phys. **131**, 244303 (2009).
[55] G. Nyman and J. Espinosa-García, J. Phys. Chem. A **111**, 11943 (2007).
[56] D. Wang and G. Czakó, J. Phys. Chem. A **117**, 7124 (2013).
[57] J. Palma and U. Manthe, J. Chem. Phys. **137**, 044306 (2012).
[58] T. Westermann, J. B. Kim, M. L. Weichman, C. Hock, T. I. Yacovitch, J. Palma, D. M. Neumark, and U. Manthe, Angew. Chem., Int. Ed. **53**, 1122 (2014).
[59] T. Westermann, W. Eisfeld, and U. Manthe, J. Chem. Phys. **139**, 014309 (2013).
[60] J. Palma and U. Manthe, J. Phys. Chem. A **119**, 12209 (2015).
[61] J. Espinosa-García, J. Phys. Chem. A **120**, 5 (2016).
[62] C. Xie, B. Jiang, M. Yang, and H. Guo, J. Phys. Chem. A **120**, 6521 (2016).
[63] D. Schäpers and U. Manthe, J. Phys. Chem. A **120**, 3186 (2016).
[64] D. Skouteris, D. E. Manolopoulos, W. Bian, H. J. Werner, L.-H. Lai, and K. Liu, Science **286**, 1713 (1999).
[65] M. H. Alexander, G. Capecchi, and H. J. Werner, Science **296**, 715 (2002).
[66] M. H. Alexander, D. E. Manolopopoulos, and H. J. Werner, J. Chem. Phys. **113**, 11084 (2000).
[67] L. Che, Z. Ren, X. Wang, W. Dong, D. Dai, X. Wang, D. H. Zhang, X. Yang, L. Sheng, G. Li *et al.*, Science **317**, 1061 (2007).
[68] F. Lique, G. Li, H. J. Werner, and M. H. Alexander, J. Chem. Phys. **134**, 231101 (2011).
[69] M. Tizniti, S. D. Le Picard, F. Lique, C. Berteloite, A. Canosa, M. H. Alexander, and I. R. Sims, Nat. Chem. **6**, 141 (2014).
[70] S. M. Remmert, S. T. Banks, J. N. Harvey, A. J. Orr-Ewing, and D. C. Clary, J. Chem. Phys. **134**, 204311 (2011).
[71] J. C. Tully, J. Chem. Phys. **93**, 1061 (1990).
[72] R. Kapral and G. Cicotti, J. Chem. Phys. **110**, 8919 (1999).
[73] M. Santer, U. Manthe, and G. Stock, J. Chem. Phys. **114**, 2001 (2001).
[74] L. Raff and D. Thompson, in *Theory of Chemical Reaction Dynamics*, edited by M. Baer (CRC Press, Boca Raton, 1985), Vol. 3, pp. 1–121.